Distinct but overlapping binding sites of agonist and antagonist at the relaxin family peptide 3 (RXFP3) receptor

Lilian L. L. Wong[‡1], **Daniel James Scott**[‡§2], **Mohammed Akhter Hossain**[‡¶], **Quentin Kaas**[‖], ⬤ **K. Johan Rosengren**[**3], and ⬤ **Ross A. D. Bathgate**[‡§4]

From the ‡*Florey Institute of Neuroscience and Mental Health,* §*Department of Biochemistry and Molecular Biology,* and ¶*School of Chemistry, University of Melbourne, Parkville, Victoria 3052, Australia and the* ‖*Institute for Molecular Bioscience and* ***Faculty of Medicine, School of Biomedical Sciences, University of Queensland, Brisbane, Queensland 4072, Australia*

Edited by Henrik G. Dohlman

The relaxin-3 neuropeptide activates the relaxin family peptide 3 (RXFP3) receptor to modulate stress, appetite, and cognition. RXFP3 shows promise as a target for treating neurological disorders, but realization of its clinical potential requires development of smaller RXFP3-specific drugs that can penetrate the blood–brain barrier. Designing such drugs is challenging and requires structural knowledge of agonist- and antagonist-binding modes. Here, we used structure–activity data for relaxin-3 and a peptide RXFP3 antagonist termed R3 B1–22R to guide receptor mutagenesis and develop models of their binding modes. RXFP3 residues were alanine-substituted individually and in combination and tested in cell-based binding and functional assays to refine models of agonist and antagonist binding to active- and inactive-state homology models of RXFP3, respectively. These models suggested that both agonists and antagonists interact with RXFP3 via similar residues in their B-chain central helix. The models further suggested that the B-chain Trp[27] inserts into the binding pocket of RXFP3 and interacts with Trp[138] and Lys[271], the latter through a salt bridge with the C-terminal carboxyl group of Trp[27] in relaxin-3. R3 B1–22R, which does not contain Trp[27], used a non-native Arg[23] residue to form cation–π and salt-bridge interactions with Trp[138] and Glu[141] in RXFP3, explaining a key contribution of Arg[23] to affinity. Overall, relaxin-3 and R3 B1–22R appear to share similar binding residues but may differ in binding modes, leading to active and inactive RXFP3 conformational states, respectively. These mechanistic insights may assist structure-based drug design of smaller relaxin-3 mimetics to manage neurological disorders.

Relaxin-3 is the most recently identified member of the relaxin peptide family and is a neuropeptide highly expressed in the brain. It was discovered in 2002 based on a search of the human genome database (1), and subsequently homologs of the relaxin-3 gene (*RLN3*) were found in other species, such as mouse, rat, pig, frog, chimpanzee, and macaque, and orthologs of relaxin-3 were found in fish, such as the Fugu (*Takifugu rubripes*) and zebrafish (*Danio rerio*) (2). Relaxin family peptides bind to class A G protein– coupled receptors known as the relaxin family peptide (RXFP)[5] receptors (3). The relaxin family peptides are part of the insulin peptide superfamily (4) and share structural homology with two peptide chains, A and B, cross-linked by three disulfide bonds: two interchain disulfide bonds between the A- and B-chain and one intrachain disulfide bond in the A-chain (4, 5). The endogenous receptor for relaxin-3 is RXFP3 (6) and was previously known as GPCR135 or somatostatin and angiotensin-like peptide receptor (SALPR) (3, 6, 7). Relaxin-3 can also bind to RXFP1 (8) and RXFP4 (9, 10), the endogenous receptors for relaxin-2 (also known as just "relaxin") and insulin-like peptide 5 (INSL5), respectively.

Relaxin-3 is highly expressed in the brains of all species where the gene has been identified, including zebrafish (11), mouse (1), rat (12), macaque (13, 14), and humans (6). Extensive studies in mice and rats have determined high levels of relaxin-3 expression in the ventromedial dorsal tegmental area also known as the nucleus incertus (NI) (1, 12, 15–17). Its high expression and extensive overlap of relaxin-3– containing fibers with the expression of RXFP3 in certain areas of the brain suggests that relaxin-3 has distinct and important functional roles (1, 17, 18). Indeed, relaxin-3 has been shown to be involved in a wide range of behaviors, which include spatial learning and memory (19); modulation of stress, mood, and arousal (20, 21); feeding and appetite (22); and addiction (23). The importance of the relaxin-3/RXFP3 system suggests that its receptor is a highly relevant target for developing receptor-specific drugs to treat neurological diseases.

⬙ASBMB

J. Biol. Chem. (2018) 293(41) 15777–15789   **15777**

Mechanism of agonist and antagonist interaction at RXFP3

Numerous studies have been focused on understanding structure activity relationship of relaxins (24). The relaxin-3 B-chain alone is capable of interacting with RXFP3, suggesting that the A-chain of relaxin-3 is not crucial for RXFP3 interactions (6, 25). Studies using a recombinant expression system to generate chimeric peptides consisting of A-chains from other relaxin family peptides together with the relaxin-3 B-chain demonstrated that a peptide consisting of the INSL5 A-chain and relaxin-3 B-chain (R3/I5) was a selective agonist for RXFP3 over RXFP1 (26). The NMR solution structures of native relaxin-3 and this chimera revealed that the center of the B-chain adopts a helical conformation (27, 28). The helix is important for activity, and recently, Hojo *et al.* (29) and Jayakody *et al.* (30) showed that hydrocarbon stapling on the B-chain of relaxin-3 can produce relaxin-3 single-chain analogs that retain potent agonist activity. NMR analysis highlighted that the stapled peptide mimicked the α-helical structure of the relaxin-3 B-chain (29) and further demonstrated that the B-chain is solely responsible for binding and activation of RXFP3. These studies demonstrate that the A-chain of relaxin-3 is not involved in binding or activation of RXFP3, and its role is to provide a scaffold for maintaining the helical structure within the B-chain. Mutagenesis studies of the B-chain in relaxin-3 led to the identification of the key amino acid residues for receptor binding on the B-chain central α helix (Arg[B12], Ile[B15], Arg[B16], Ile[B19], and Phe[B20]), whereas the amino acid residues Arg[B26] and Trp[B27] at the C terminus make only a minor contribution to binding affinity but are essential for receptor activation (Fig. 1, *A* and *B*) (31).

Truncation of the C terminus of the B-chain led to the generation of an RXFP3 antagonist. Interestingly, the addition of a non-native arginine after Cys[B22] at the C terminus, as a result of an artifact of the recombinant production and processing, in the peptide R3(BΔ23–27)R/I5 increased the affinity for RXFP3 (31). A further study showed that the additional arginine is a major contributor for the high-affinity binding of R3(BΔ23–27)R/I5 to RXFP3 (32). The introduction of this amino acid residue has been suggested to provide an additional binding interaction that compensates for the reduction in affinity from the loss of the C-terminal amino acid residues (32). Subsequently, a single-chain variant of this truncated peptide with the cysteine residues mutated to serine was developed. This variant, R3 B1–22R (Fig. 1C), is also a high-affinity RXFP3 antagonist and, furthermore, does not have any affinity for the RXFP4 or RXFP1 receptors and thus is RXFP3-specific (33). Importantly, this peptide is unstructured in solution, and the Arg[23] residue is important for the high-affinity binding, as the variant lacking this arginine demonstrated no binding to RXFP3 (33).

Knowledge of the precise agonist and antagonist binding sites on RXFP3 would further assist the structure-based design of drug leads. Despite having a good understanding of the important B-chain amino acid residues that are responsible for the activity of relaxin-3, little is known about the amino acid residues in RXFP3 that they are interacting with. Mutagenesis studies on RXFP3 together with molecular modeling and ligand docking demonstrated that Arg[B12] and Arg[B16] are likely interacting with Glu[244] in extracellular loop 2 (EL2) and Asp[145] in
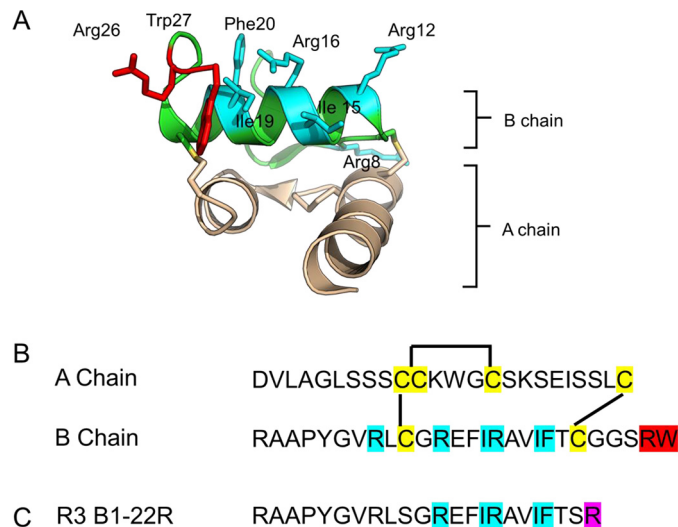

Figure 1. *A*, NMR solution structure of relaxin-3 (PDB entry 2FHW). The key amino acid residues (shown as *sticks*) involved in binding are shown in *cyan*, and those involved in activation are shown in *red*. Relaxin-3 A-chain is *colored* in *wheat*, whereas the B-chain is *colored* in *green*. The C terminus of the relaxin-3 B-chain folds back to interact with the α-helical core residues. *B*, peptide sequence of human relaxin-3 with the amino acid residues important for binding *highlighted* in *cyan*, residues involved in activation *highlighted* in *red*, and the cysteine residues forming disulfide bonds *highlighted* in *yellow*. *C*, peptide sequence of R3 B1–22R with the binding residues utilized by relaxin-3 *highlighted* in *cyan*, whereas Arg[23], *highlighted* in *magenta*, is a non-native residue shown to be very important for binding to RXFP3.

EL1, respectively, whereas Arg[B26], one of the critical amino acid residues for activating the receptor, is interacting with Glu[141] in transmembrane domain 2 (TM2) (Fig. 2A) (34, 35). However, the interaction sites for the hydrophobic amino acid residues, Ile[B15], Ile[B19], Phe[B20], and Trp[B27], with the receptor are still unknown. A further study using RXFP3 mutagenesis hypothesized that Trp[B27] interacts with Trp[138] in RXFP3 after a conformational change of the C terminus of the peptide upon binding the receptor (36). Importantly, there is no information as to the amino acid residues that bind the RXFP3-specific antagonist R3 B1–22R, particularly the non-native arginine Arg[23] on its C terminus, which is the largest contributor to its affinity. Given the prominent neurological effects following the activation and inhibition of RXFP3 signaling in the brain, RXFP3 presents immense potential as a drug target to treat neurological disorders. Designing small, receptor-specific drugs that can penetrate the blood–brain barrier is challenging and requires understanding of the molecular details of the ligand–receptor complex and the conformational changes that occur upon activation. In the present study, we investigated the roles of several amino acid residues in RXFP3 that we predicted might be interacting with relaxin-3 and the R3 B1–22R single-chain antagonist. Using site-directed mutagenesis, we studied the effects of mutating these amino acid residues on both agonist and antagonist binding as well as the effects of mutations on the activation of RXFP3 following agonist stimulation. Based on these data, we present detailed models of the agonist and antagonist binding sites of RXFP3 and new mechanistic insights into its function.
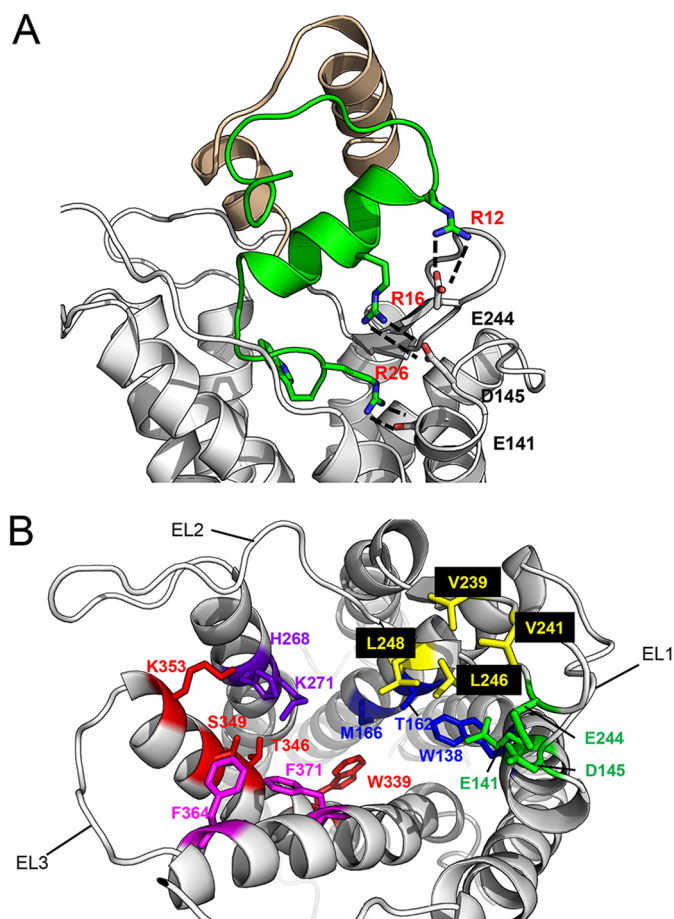
Figure 2. Rational predictions of RXFP3 mutations guided by our previous homology model generated based on the inactive structure of CXCR4. *A*, model of the relaxin-3–RXFP3 complex showing the electrostatic interactions between the positively charged arginines Arg[B12], Arg[B16], and Arg[B26] (*labeled* in *red*) of relaxin-3 B-chain (*green*) and the negatively charged Glu[244], Asp[145], and Glu[141], respectively. *B*, extracellular view of the homology model of RXFP3–relaxin-3 complex with relaxin-3 removed to provide a clearer view. Amino acid residues rationalized to be interacting with relaxin-3 are shown in *sticks* and *color-coded* accordingly. Residues in TM2 and TM3 are shown in *blue* and residues in EL2, TM5, TM6, and TM7 are shown in *yellow*, *purple*, *red*, and *pink*, respectively.

Results and discussion

Predictions of relaxin-3/RXFP3 interactions

In previous studies exploring the role of acidic amino acid residues in RXFP3 for relaxin-3 binding, interaction partners for the key basic amino acid residues in relaxin-3, Arg[B12], Arg[B16], and Arg[B26], were identified (34, 35) (Fig. 2A). These interactions suggest that the relaxin-3 B-chain C terminus inserts into the RXFP3 binding pocket, whereas the B-chain helical region primarily packs against EL2. To further confirm and refine the model of ligand binding and to also identify hydrophobic amino acid residues in RXFP3 that are interacting with the remaining amino acid residues critical for bioactivity (Ile[B15], Ile[B19], Phe[B20], and Trp[B27]), we designed a new set of rationally predicted RXFP3 mutations based on the proximities of ligand to receptor residues generated from our docking studies of relaxin-3 on the RXFP3 homology model (Fig. 2B) that we created in our previous study (34). Based on the model, Ile[B15] and Ile[B19] are exposed on a surface of the B-chain helix adjacent to an RXFP3 hydrophobic patch that includes Val[239], Val[241],

Leu[246], and Leu[248] in EL2; thus, these were mutated to alanine (Fig. 2B). Phe[B20] is exposed on a different face of the helix and is observed to be in close proximity to another bulky residue on TM7, Phe[364], which was therefore also mutated to alanine (Fig. 2B). Finally, the C terminus of the B-chain is rather flexible, and a conformational change has been suggested (35), meaning there are a number of potential interaction partners for Trp[B27], including Trp[138] in TM2; Thr[162] and Met[166] in TM3; His[268] and Lys[271] in TM5; Trp[339], Thr[346], Ser[349], and Lys[353] in TM6; and Phe[371] in TM7 (Fig. 2B). These amino acid residues were also all individually mutated to alanine. The combination of these mutations represents an extensive exploration of a large portion of the RXFP3 ligand-binding pocket (Fig. 2B).

Effect of mutagenesis on agonist binding to RXFP3

A total of 15 mutations were generated based on their proximity to key relaxin-3– binding residues. The mutants were first tested for changes in agonist binding in cell-based binding assays using europium-labeled (Eu-)R3/I5. Receptor mutants were tested in parallel for their cell surface expression, and the final specific binding data were expressed as a ratio of the percentage of specific binding/cell surface expression. Eight of 15 mutations tested (W138A (TM2); T162A (TM3); V241A, L246A, and L248A (EL2); K271A (TM5); and F364A and F371A (TM7)) resulted in a significant loss (~70 – 85% compared with WT) in Eu-R3/I5–specific binding without affecting receptor cell surface expression (Fig. 3 and Table 1). Other mutations, such as V239A (EL2), W339A, T346A, S349A, and K353A (TM6) had no effect on binding or cell surface expression (Fig. 3 and Table 1). On the other hand, M166A (TM3) and H268A (TM5) showed increased specific agonist binding despite having normal cell surface expression (Fig. 3 and Table 1). The mutation of the bulky side chains of histidine and methionine to alanine may free up steric constraints in the binding pocket and hence the observed higher specific binding. Additionally, His[268] is positioned one helix turn above Lys[271], which showed affected agonist binding, and hence the removal of the His[268] side chain may open up the binding pocket.

Activation of mutant RXFP3 receptors

RXFP3, when activated by agonists, couples to $G_{i/o}$ proteins to inhibit cAMP production. To assess the ability of the mutant receptors to signal, we therefore used a pCRE-β-gal reporter gene assay, which is an indirect readout of cAMP activity and has been extensively utilized to assess agonist activity at RXFP3 (33, 37). When the mutant receptors were tested in cAMP activity assays, 9 of 15 mutations demonstrated significantly reduced agonist potency (pEC$_{50}$) compared with WT RXFP3 (Fig. 4 and Table 1). Notably, there were no changes in ligand-activated efficacy for all of the mutations where a full-dose response was demonstrated. For the mutants where there was not a full-dose response (W138A, L248A, K271A, W339A, and F371A), efficacy values at 1 μM agonist were shown, and potencies were described as <6 (Table 1). Seven of the 9 mutations (W138A, T162A, L246A, L248A, K271A, F364A, and F371A) previously showed decreased specific binding (Fig. 4 (*A and B*), Fig. S1, and Table 1). Mutations at W138A, K271A, F371A, and L248A were particularly detrimental for activation, resulting in
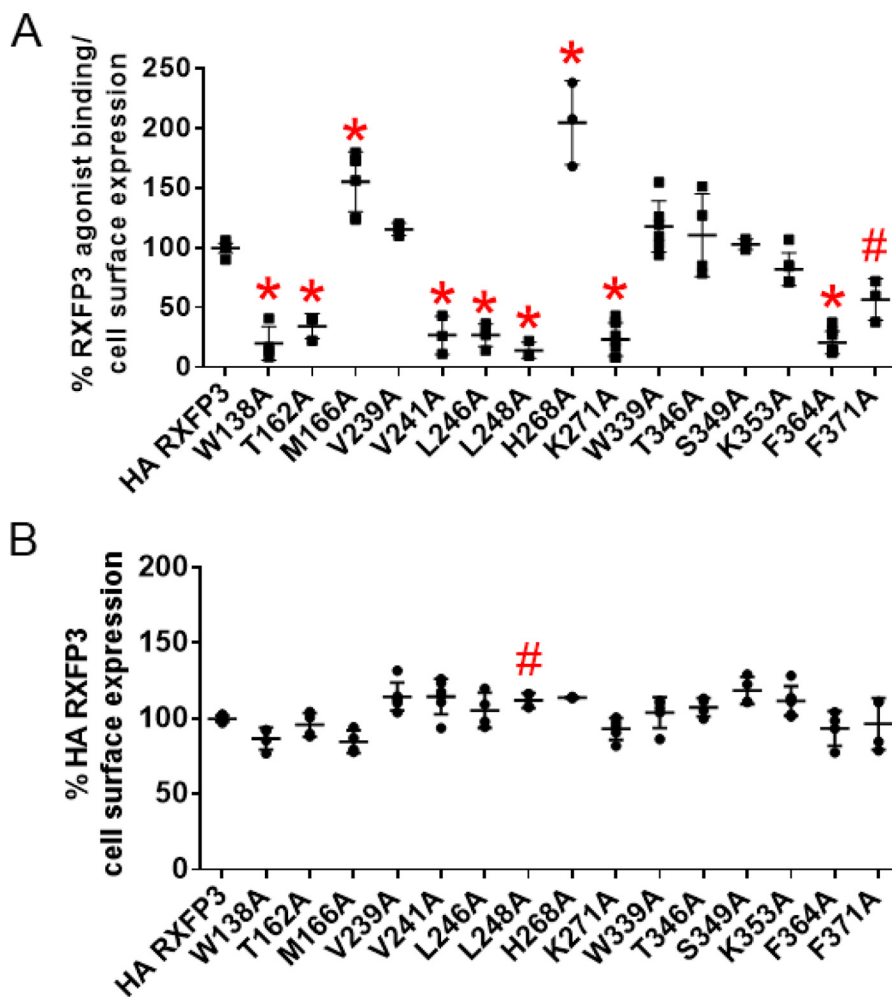
SASBMB

Figure 3. *A*, Eu-R3/I5–specific binding to mutant RXFP3 receptors compared with HA-RXFP3. Data are expressed as a ratio of specific Eu-R3/I5 binding to the cell surface expression of each construct and normalized to HA-RXFP3 binding. *B*, cell surface expression of HA-tagged receptors compared with WT HA-RXFP3. Data are expressed as mean $\pm$ S.D. (*error bars*) of triplicate measurements from at least three independent experiments ($n = 3$–8; *, $p < 0.001$; #, $p < 0.05$ *versus* HA-RXFP3).

more than 1000-fold lower agonist potency compared with WT RXFP3, which suggest that these amino acid residues may be involved in agonist recognition (Fig. 4 (*A* and *B*), Fig. S1, and Table 1). Interestingly, W339A and T346A, which did not show any significant decrease in specific agonist binding, demonstrated significant losses in cAMP activity, suggesting their roles in stabilizing the active conformation instead of a direct role in ligand recognition (Figs. 3*A* and 4*B*, Fig. S1, and Table 1). In particular, W339A demonstrated minimal activity (~30% efficacy; Table 1) to agonist at concentrations up to 1 μM, suggesting that this amino acid residue is probably important for stabilizing the active receptor conformation, and mutations to alanine shift the receptor toward the inactive state. Indeed, Trp[339] or W6.48 (according to the Ballesteros–Weinstein numbering scheme (38)), which is located on the CW*X*P motif that is widely known as the "rotamer toggle switch," is important for activation (39, 40). Mutagenesis studies of W6.48 in A₃ adenosine receptor, GPR119, GPR39, NK1, and the β₂-adrenergic receptor demonstrated that mutation of this amino acid residue significantly affected agonist-induced receptor activation but did not impair agonist affinity (41, 42). The other four mutations (T162A, L246A, T346A, and F364A) had significantly

lower agonist potency but showed a less dramatic drop (Fig. 4*B*, Fig. S1, and Table 1). In contrast, V241A, which had a dramatic loss in specific agonist binding, did not show impairment in cAMP signaling (Fig. 4*A* and Table 1).

Refined model of the RXFP3–relaxin 3 complex

In our previous study (34), we generated a homology model of RXFP3 and performed ligand-docking simulations guided by our mutagenesis data based on the inactive structure of the CXCR4 receptor (PDB entry 3OEO (43)). We have utilized this model to predict further interaction sites and perform more RXFP3 alanine mutations in this study. Recently, the active (44) and inactive (45) structures of the angiotensin II receptor type I, which shares higher homology with RXFP3, became available, which allowed us to use these structures as templates for the homology modeling of active and inactive RXFP3 models to refine docking based on our current mutagenesis and peptide SAR data (see companion paper (59)). Based on these results, we further refined our model of how relaxin-3 binds and activates RXFP3 (Fig. 5*A*). The importance of Leu[246] and Leu[248] strongly supports a binding mode that places Ile[B15] and Ile[B19] packed against the small β-sheet in EL2 with hydrophobic

Table 1

Summary table of the binding and activity data of the mutant receptor constructs compared with WT receptor (HA-RXFP3)

The number of experimental replicates for each mutant receptor is shown in parentheses with the reported data shown as mean ± S.E. *, $p < 0.001$; **, $p < 0.01$; #, $p < 0.05$ compared with HA-RXFP3. ND, not determined.

| Mutation	Position	Cell surface expression	Agonist			Antagonist		
			Specific binding	pEC50 activity	Efficacy	Specific binding	K_d	B_{max}
		% HA RXFP3	% HA RXFP3		% inhibition	% HA RXFP3	nM	% HA RXFP3
HA-RXFP3		100.00 ± 0.73 (8)	99.23 ± 1.67 (8)	8.91 ± 0.06 (9)	67.74 ± 5.40 (9)	100.00 ± 2.34 (6) (6) (10)	30.49 ± 0.97 (19)	100 (19)
E141A	EL1	111.70 ± 1.20 (3)	1.47 ± 0.37 (4)*	No activity (3)	No activity (3)	24.61 ± 4.05 (5)*	>100	ND
D145A	EL1	105.59 ± 2.67 (3)	9.99 ± 0.91 (4)*	7.52 ± 0.23 (3)*	49.07 ± 7.92 (3)	29.55 ± 3.86 (5)*	>100	ND
E141A/D145A	EL1	118.80 ± 1.18 (3)	6.79 ± 1.48 (4)*	No activity (3)	No activity (3)	25.24 ± 3.55 (3)*	>100	ND
E244A	EL2	84.11 ± 4.35 (4)	20.20 ± 4.35 (4)	8.01 ± 0.03 (3)*	53.66 ± 5.31 (3)	35.82 ± 6.31 (3)*	50.47 ± 1.67 (5)*	78.83 ± 4.44 (5)
E245A	EL2	39.43 ± 2.33 (3)*	50.46 ± 2.33 (3)*	ND	ND	91.07 ± 9.63 (3)	32.86 ± 7.22 (5)	49.86 ± 4.55 (3)*
E141A/W138A	EL1	102.93 ± 5.73 (3)	ND	ND	ND	No binding	>100	ND
W138A	TM2	86.78 ± 3.65 (4)	20.22 ± 5.47 (5)*	<6 (3)	29.75 ± 2.83 (3) (3)**	30.54 ± 4.09 (5)*	42.13 ± 3.21 (3)	87.15 ± 6.72 (3)
T162A	TM3	95.84 ± 4.00 (4)	34.24 ± 3.25 (4)*	7.79 ± 0.04 (3)* (3)**	73.42 ± 3.08 (3)	30.56 ± 4.86 (3)	29.38 ± 1.90 (3)	86.44 ± 3.16 (3)
M166A	TM3	81.42 ± 3.73 (4)	151.33 ± 8.49 (7)*	8.72 ± 0.02 (3)	74.46 ± 3.46 (3)	103.90 ± 0.96 (3)	ND	ND
V239A	EL2	114.49 ± 3.79 (3)	112.2 ± 4.77 (4)	9.39 ± 0.15 (3)	67.85 ± 1.69 (3)	92.87 ± 5.44 (4)	39.91 ± 0.69 (3)	105.08 ± 10.43 (3)
V241A	EL2	114.59 ± 4.74 (3)	114.59 ± 4.74 (3)	8.80 ± 0.04 (3)	68.88 ± 5.63 (3)	52.04 ± 2.63 (5)*	60.20 ± 1.91 (4)*	131.95 ± 17.90 (4)
L246A	EL2	105.48 ± 5.76 (4)	105.48 ± 5.76 (4)	7.30 ± 0.39 (3)*	74.32 ± 5.44 (3)	45.91 ± 3.80 (5)*	70.98 ± 8.89 (5)*	101.26 ± 3.52 (5)
L248A	EL2	112.08 ± 2.46 (4)	112.08 ± 2.46 (4)	<6 (3)	53.56 ± 1.76 (3)	47.96 ± 2.56 (4)*	84.56 ± 8.70 (5)*	112.41 ± 15.74 (5)
H268A	TM5	113.93 ± 0.26 (3)	215.38 ± 22.16 (4)*	8.91 ± 0.20 (3)	67.86 ± 6.23 (3)	53.00 ± 4.44 (3)*	52.43 ± 4.39 (4)**	95.26 ± 9.49 (4)
K271A	TM5	89.56 ± 4.93 (4)	21.57 ± 2.97 (7)*	<6 (5)	20.00 ± 3.50 (5)*	74.13 ± 6.29 (3)*	32.84 ± 5.97 (3)	85.05 ± 6.78 (3)
W339A	TM6	93.90 ± 3.91 (4)	107.55 ± 8.32 (7)	<6 (5)	29.30 ± 5.25 (5)*	84.56 ± 13.36 (5)	75.56 ± 5.90 (5)*	125.12 ± 10.83 (5)
T346A	TM6	113.66 ± 4.45 (3)	110.36 ± 10.77 (4)*	7.58 ± 0.12 (3)*	71.46 ± 13.37 (3)	45.72 ± 5.48 (3)	58.45 ± 3.81 (4)*	99.68 ± 8.70 (4)
S349A	TM6	99.84 ± 11.27 (3)	105.40 ± 7.45 (4)	8.78 ± 0.04 (3)	63.81 ± 4.38 (3)	49.48 ± 5.48 (3)	25.71 ± 2.08 (4)	86.84 ± 1.51 (4)
K353A	TM6	119.68 ± 8.91 (4)	97.73 ± 9.63 (7)	8.73 ± 0.26 (4)	63.77 ± 5.14 (4)	93.76 ± 5.74 (6)	60.12 ± 3.56 (4)*	92.07 ± 8.05 (4)
F364A	TM7	86.83 ± 5.52 (4)	20.52 ± 2.74 (7)*	7.30 ± 0.05 (4)* (4)*	74.31 ± 5.96 (4)	49.40 ± 6.59 (3)*	16.84 ± 1.09 (3)	99.50 ± 1.40 (3)
F371A	TM7	96.44 ± 8.55 (3)	66.47 ± 10.5 (3)*	<6 (3)	43.98 ± 7.38 (3)*	111.42 ± 11.40 (3)		
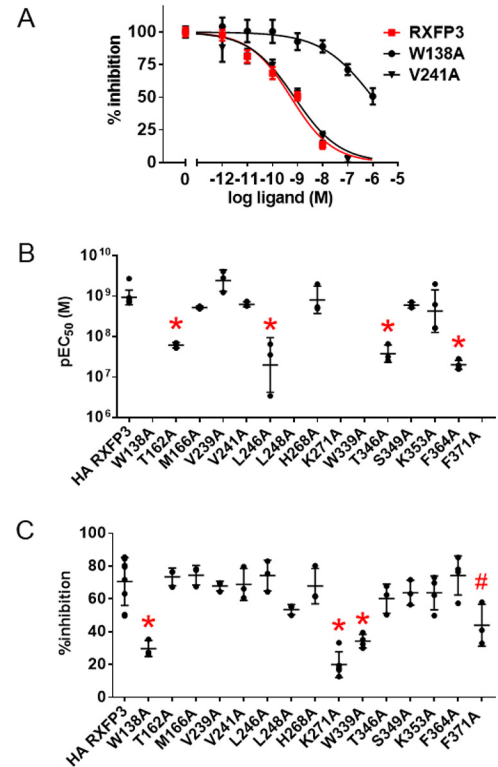
Figure 4. Characterization of mutant receptors in a pCRE-β-gal reporter gene assay in transiently transfected HEK293T cells. *A*, representative dose-response curves for W138A in TM2, a mutation that disrupted signaling, and V241A in EL2, a mutation that did not affect signaling. All individual dose-response curves of mutant RXFP3 receptors are shown in Fig. S2. *B* and *C*, the pEC50 (*B*) and efficacy of the inhibition (*C*) of forskolin-stimulated cAMP accumulation when stimulated with the RXFP3 full agonist, analogue 2, at the HA-RXFP3 and mutant RXFP3 receptors. Data are expressed as mean ± S.D. (*error bars*) of triplicate measurements from at least three independent experiments ($n = 3$–9; *, $p < 0.001$; #, $p < 0.05$ compared with HA-RXFP3). pEC50 and efficacy values are summarized in Table 1.

interactions between Ile[B15] and Leu[246] and between Ile[B19] and Leu[248] (Fig. 5B). Ile[B15] has been shown to be critical for relaxin-3 binding previously (31) with an alanine replacement of this amino acid residue resulting in a dramatic loss of affinity for RXFP3. Replacement of Ile[B19] with alanine only shows a moderate drop in affinity, but replacement with a charged amino acid residue (glutamic acid) is detrimental, confirming the importance of a hydrophobic nature at this position (31). The V239A replacement in RXFP3 was well tolerated, suggesting that this amino acid residue is outside the binding site. V241A, despite showing a significant drop in Eu-R3/I5 binding, did not show impairment in signaling, suggesting that it may only make a minor contribution to binding affinity.

Trp[B27] was positioned in our preliminary model toward TM5 and TM6, based on the preferred conformation of this amino acid residue in the relaxin-3 solution NMR structure. However, of the amino acid residues mutated in this region (Thr[162], His[268], Lys[271], Trp[339], Thr[346], Ser[349], Lys[353] and Phe[371]), only Thr[162], Lys[271], and Phe[371] were found to be important for RXFP3 binding and activation. NMR studies on relaxin-3 peptide have suggested a degree of flexibility afforded by the Gly–Gly hinge between the binding and activation domains, and such a rearrangement has previously been proposed to allow for receptor activation, as mutation of the flexible Gly-Gly to Ala-
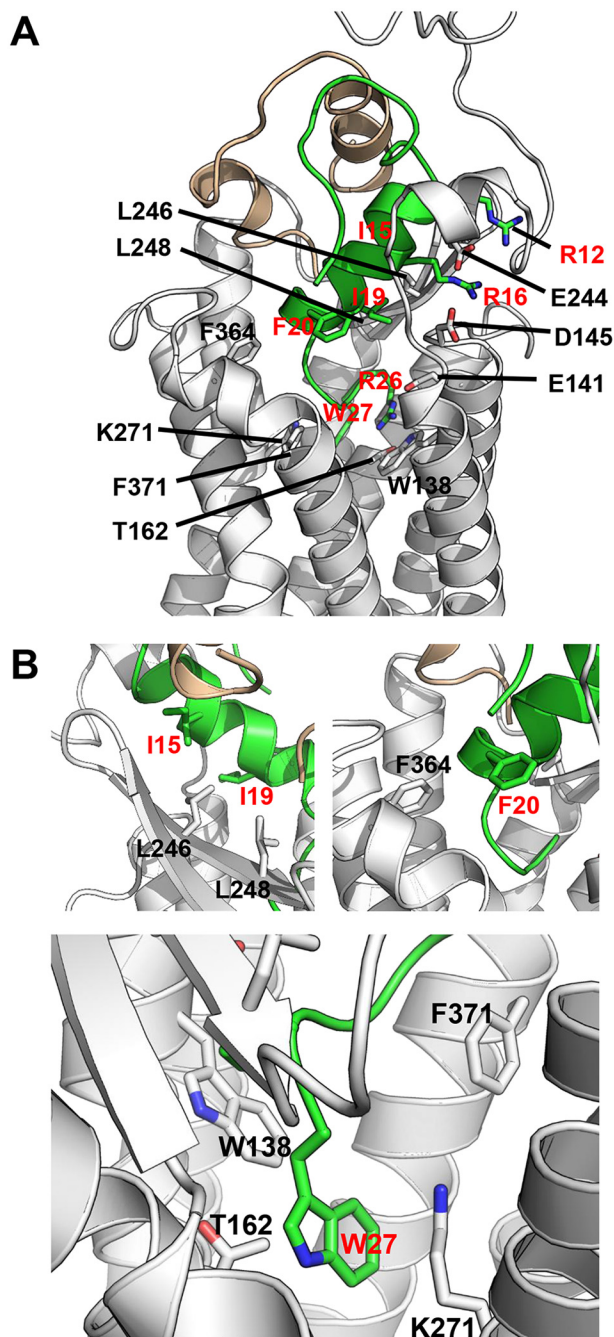
Figure 5. *A*, relaxin-3 docked into an active-state homology model of RXFP3 (*gray*) with amino acid residues predicted to be interacting shown as *sticks*. *B*, *close-up* of the predicted interactions between hydrophobic residues Ile^{B15} and Ile^{B19} on relaxin-3 with Leu^{246} and Leu^{248} in EL2 of RXFP3, Phe^{B20} with Phe^{364} in TM7 of RXFP3 and Trp^{B27} of the flexible C terminus with several amino acid residues in TM2 (Trp^{138}), TM3 (Thr^{162}), TM5 (Lys^{271}), and TM7 (Phe^{371}). Ligand and receptor amino acid residues involved in interactions are labeled in *red* and *black*, respectively.

same time this work was undertaken, the Trp^{B27} interaction with Trp^{138} on TM2 was also demonstrated by Hu *et al.* (36), showing that the mutant W138A was not able to discriminate between relaxin-3 and a variant lacking Trp^{B27}. Considering that the C terminus is flexible and Trp^{B27} is a large amino acid residue, the effects of mutations to Thr^{162} and Phe^{371} in its proximity are also likely a result of either direct interactions or indirect local conformational changes that affect its binding pocket (Fig. 5*B*).

In the model, Phe^{B20} is located on the other face of the relaxin-3 B-chain helix and thus does not appear to be able to interact with EL2. Instead, we speculated that through a small rotation, it could contact amino acid residues on the opposite side of the binding site. It was previously shown that the replacement of Phe^{B20} with alanine showed only a moderate drop in affinity, but a replacement with a charged arginine or a polar group like serine resulted in a significant affinity drop, suggesting that the nature of the Phe^{B20} interactions is hydrophobic (31). Indeed, when Phe^{B20} was replaced with a hydrophobic and bulky tyrosine, the affinity of the peptide was rescued (31). A mutation to Phe^{364} in TM7 was used to probe this possibility, and the variant F364A showed reduced agonist binding and RXFP3 activation; thus, we propose that it is interacting with relaxin-3 Phe^{B20} (Fig. 5*B*).

Effect of mutagenesis of acidic residues on antagonist binding in RXFP3

Little is known about how the single-chain antagonist R3 B1−22R interacts with RXFP3. Given that all features of the helical portion of the B-chain are retained, key amino acid residues in this region might be involved in similar interactions as in relaxin-3. However, unlike relaxin-3, R3 B1−22R lacks the C-terminal Arg^{B26} and Trp^{B27} interaction sites but gains an additional high-affinity binding site through the non-native C-terminal Arg^{23}. In addition, it is known that R3 B1−22R with a C-terminal acid binds with lower affinity compared with a C-terminal amide (33). On the other hand, for relaxin-3, a B-chain C-terminal acid is required for high affinity and activity (47). Therefore, we would predict that there are some distinct differences in the binding mode compared with relaxin-3 due to the critical new interactions introduced by the non-native Arg^{23} and the C-terminal amide (see companion paper (59)). As the unstructured antagonist must still partially rely on the binding amino acid residues of relaxin-3, we hypothesized that R3 B1−22R formed a helical structure upon the first contact with the receptor, which is primarily driven by Arg^{23}, subsequently allowing other binding amino acid residues on the central region of R3 B1−22R to interact with RXFP3. Given the involvement of positively charged arginines in the ligand (see companion paper (59)), we first screened binding to acidic mutant receptors to analyze whether these are involved in similar interactions as with relaxin-3.

All of the acidic mutant receptors except E245A have been previously shown not to affect receptor cell surface expression (34). E245A, which is pointing away from the binding site in our model, has impaired cell surface expression (34) (∼40% of WT) but importantly has unchanged affinity for R3 B1−22R (Fig. 6*A*) but reduced maximum binding, as expected (Fig. S2 and Table 1). Both

Ser resulted in a dramatic drop in relaxin-3 activation potency (46). The strong dependence of Trp^{138} on binding instead suggested that the Trp^{B27} aromatic ring in relaxin-3 is stacked against TM2. This, in turn, places the Trp^{B27} C terminus in a position to be able to form a salt bridge across the binding pocket to the extended side chain of Lys^{271} (Fig. 5*B*), an interaction that would explain the importance of both Lys^{271} and a free acid at the C terminus for maximal activity (47). At the

ASBMB

E244A and D145A, however, demonstrated reduced affinity for R3 B1–22R (Fig. 6 (*A* and *B*), Fig. S2, and Table 1), consistent with our hypothesis that they, as in relaxin-3, interact with Arg[12] and Arg[16]. R3 B1–22R lacks the C terminus of relaxin-3, but we predicted that if both the agonist and the antagonist interact with RXFP3 using similar residues, this would mean that R3 B1–22R Arg[23] could bind close to the amino acid residues interacting with Arg[B26] and Trp[B27] of the agonist. Interestingly, E141A also demonstrated reduced affinity for R3 B1–22R (Fig. 6*B* and Table 1), although its interaction partner Arg[B26] of relaxin-3 is missing in R3 B1–22R. Additionally, the combination of E141A/D145A further decreased the affinity (Fig. 6*B* and Table 1). Notably, the double mutant was still able to bind R3 B1–22R, but we were not able to obtain an affinity that was >100 nM. Thus, Arg[23] could potentially be interacting with Glu[141]. However, as the removal of Arg[23] from the R3 B1–22R completely abolishes binding of the antagonist peptide, we would have anticipated a complete loss of binding if its binding partner was removed from the receptor. Hence, at this point, we hypothesize that Glu[141] is most likely not the only amino acid residue that is interacting with Arg[23].

Effect of mutagenesis of nonacidic residues on antagonist binding in RXFP3

Given the involvement of Glu[244] and Asp[145], we predicted that the hydrophobic patch on EL2 of RXFP3 could also retain interactions with Ile[15] and Ile[19] of R3 B1–22R, as for relaxin-3. To test this and further characterize the binding mode, we tested all of the nonacidic mutant receptors for antagonist binding. W138A, V241A, L246A, L248A, K271A, and F364A, which affected agonist binding, also significantly decreased the R3 B1–22R binding, albeit to a lesser extent than agonist binding (Fig. 6*C* and Table 1). Because we observed more subtle changes in specific binding, we performed full saturation binding on these mutant receptors. W138A showed a pronounced loss in binding affinity characterized in Eu-R3 B1–22R saturation binding (Fig. 6*D*). L246A, L248A, K271A, and F364A had a moderate (~2-fold) but significant decrease in K_d (Fig. S2 and Table 1), whereas V241A did not show any perturbations in binding R3 B1–22 R as compared with WT (Fig. S2 and Table 1). H268A, T346A, and S349A resulted in a decrease in antagonist affinity (~2–3-fold) but not agonist binding or potency, suggesting that these amino acid residues are specifically interacting only with the antagonist (Fig. 6*C*, Fig. S2, and Table 1). On the other hand, K271A, which demonstrated decreased agonist binding and potency, did not significantly impair antagonist binding (Fig. S2 and Table 1). Although K271A showed slightly reduced (~75% of WT binding) antagonist binding, this was not significantly different compared with WT ($p > 0.05$). However, saturation binding on K271A indicated a slight reduction in antagonist affinity (Fig. S2 and Table 1). There was no change in B_{max} value for any mutant receptor other than E245A, which also showed lower cell surface binding. Taken together, this suggests that although there are overlapping binding sites common to both antagonist and the agonist, there are also distinct differences in the binding mode.

Despite the mutational data giving clear insights into the antagonist interaction, these mutations so far had not resulted in a complete loss of R3 B1–22R binding, which would be expected if the amino acid residues interacting with Arg[23] on the antagonist had been eliminated. The most plausible explanation is that Arg[23] forms complex interactions with several amino acid residues in the binding pocket, and hence, mutating a single amino acid residue does not result in a complete loss of binding. Analyzing the structural model, we predicted that Arg[23] could be forming both an ionic interaction with Glu[141] and a cation–π interaction with Trp[138]. Thus, we made the doubly mutated W138A/E141A. The W138A/E141A mutant receptor was expressed normally at the cell surface (Fig. 7*A*), but when tested in saturation binding, it resulted in a complete loss of Eu-R3 B1–22R binding (Fig. 7*B*), strongly suggesting that our hypothesized interaction with Arg[23] is correct and explaining the absolute requirement of this amino acid residue.

Distinct but overlapping binding modes of agonist and antagonist

Based on the mutagenesis data and our refined active- and inactive-state RXFP3 models, we performed docking simulations with the agonist and the antagonist to the active and inactive RXFP3 models, respectively. Our data suggest distinct but overlapping binding modes of relaxin-3 (Fig. 5*A*) and R3 B1–22R (Fig. 8*A*). Although R3 B1–22R is unstructured in solution, it likely forms a helix upon the interaction with RXFP3, which is mainly driven by the high-affinity binding of Arg[23] (see companion paper (59)). It is not uncommon for intrinsically disordered peptides that are flexible in solution to switch to a well-ordered structure upon binding to its receptor. From previous structure–activity relationship studies (31, 33), it is known that relaxin-3 utilizes binding amino acid residues on the central helix of the B-chain, such as Arg[B12], Ile[B15], Arg[B16], and Ile[B19]. In our refined models guided by mutagenesis, we postulate that these amino acid residues in both relaxin-3 and R3 B1–22R interact with amino acid residues Glu[244], Leu[246], Asp[145], and Leu[248], respectively, forming a binding surface spanning extracellular loops 1 and 2 (Figs. 5*B* and 8*A*).

For relaxin-3, the C-terminal tail with the critical Arg[B26]-Trp[B27] inserts into the binding pocket to activate the receptor. Arg[B26] forms a previously identified key ionic interaction with Glu[141]. Trp[B27] at the C terminus is a large amino acid residue, and the flexibility imparted by the Gly–Gly hinge makes predictions of its exact position and multiple interaction partners difficult. However, we have refined our models, and based on functional assays, we hypothesized that Trp[B27] stacks on Trp[138] of TM2. This is consistent with a previous study that identified Trp[138] as key amino acid residue interacting with Trp[B27] of relaxin-3, as the removal of Trp[B27] renders relaxin-3 insensitive to the alanine mutation W138A (36). Importantly, this conformational rearrangement allows the backbone carboxyl of Trp[B27] to interact with Lys[271] on the other side of the binding site, on TM5 (Fig. 5*B*). The importance of both Lys[271] and the free acid at the C terminus can thus potentially be explained by a salt bridge between these oppositely charged groups. Finally, we proposed that Phe[B20] stretches across the top of RXFP3 to
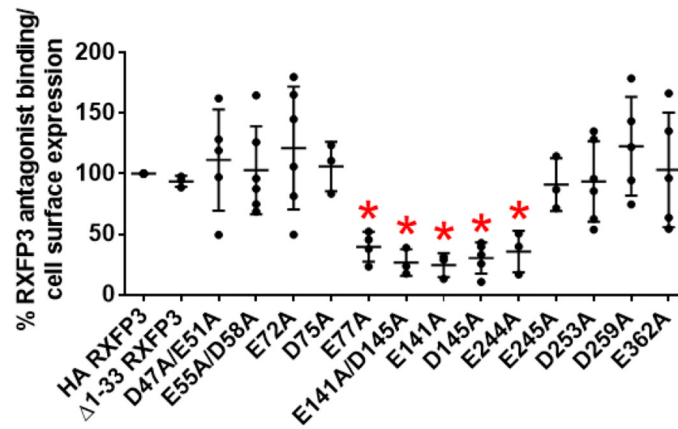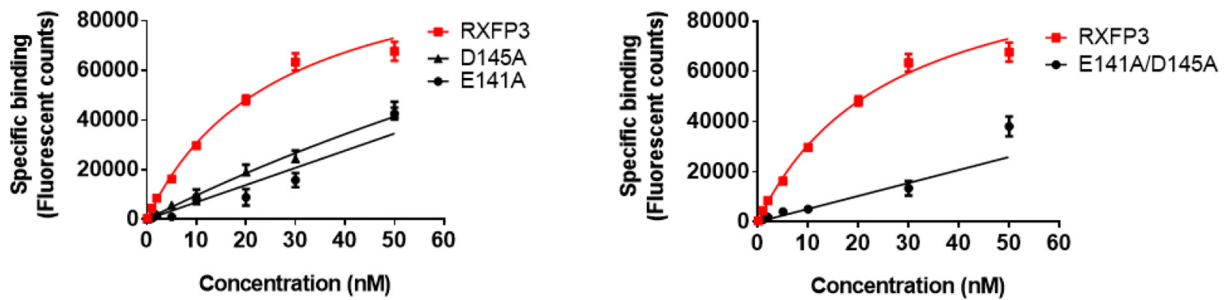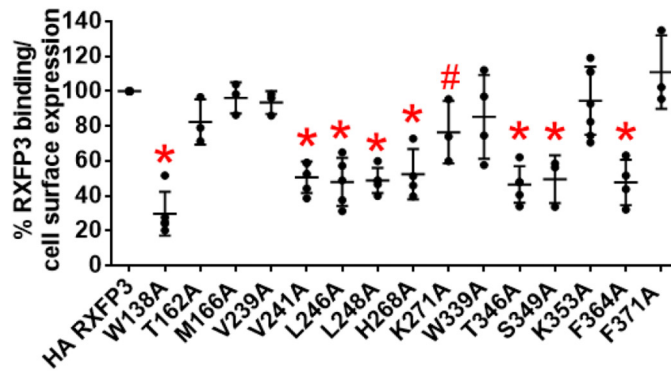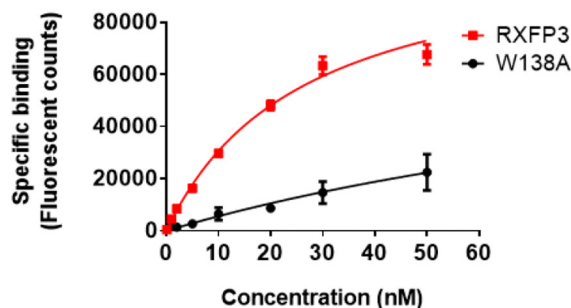
Figure 6. *A*, specific Eu-R3 B1–22R binding to RXFP3 receptors with mutations in residues predicted to be involved in electrostatic interactions with R3 B1–22R. *B*, representative Eu-R3 B1–22R saturation binding curves fit to one-site specific binding of acidic mutants E141A and D145A and double mutant E141A/D145A. All saturation binding curves for mutant receptors are shown in Fig. S2. *C*, specific Eu-R3 B1–22R binding to hydrophobic residue mutant RXFP3 receptors predicted to form hydrophobic interactions with R3 B1–22R. *D*, saturation binding of Eu-R3 B1–22R to hydrophobic W138A mutant receptor fitted to one-site specific binding. Data are expressed as mean $\pm$ S.E. (*error bars*) of triplicate measurements from at least three independent experiments ($n = 3$–19; *, $p < 0.001$; #, $p < 0.05$ compared with HA RXFP3). K_d values of mutant receptors are summarized in Table 1.

form an interaction with Phe[364]. Thus, the large relaxin-3 peptide covers the majority of the extracellular parts of the receptor, essentially forming a lid over the binding pocket, which accommodates the activation domain.

For R3 B1–22R, nothing was previously known about how the non-native Arg[23] interacted with RXFP3 to maintain RXFP3 in an inactive state. Given that Arg[23] is positively charged, we expected to easily identify a counterpart negatively
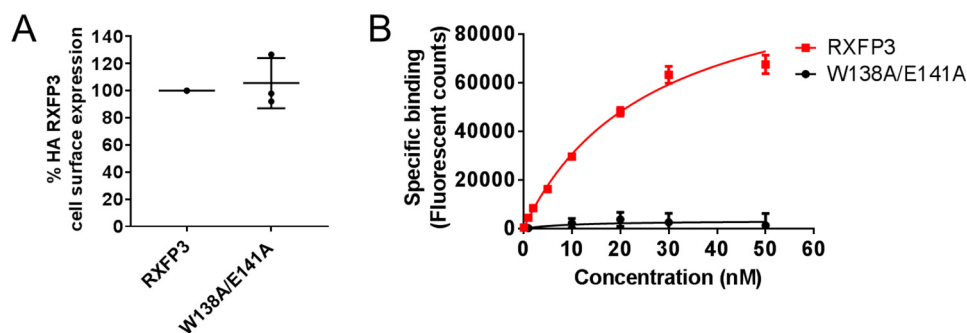
Figure 7. *A*, cell surface expression of double mutant W138A/E141A showing that the double mutant receptor is expressed at the same level as HA-RXFP3. *B*, saturation binding of Eu-R3 B1–22R on double mutant W138A/E141A demonstrates a complete loss of antagonist binding. Data are expressed as mean ± S.E. (*error bars*) of triplicate measurements from at least three independent experiments.
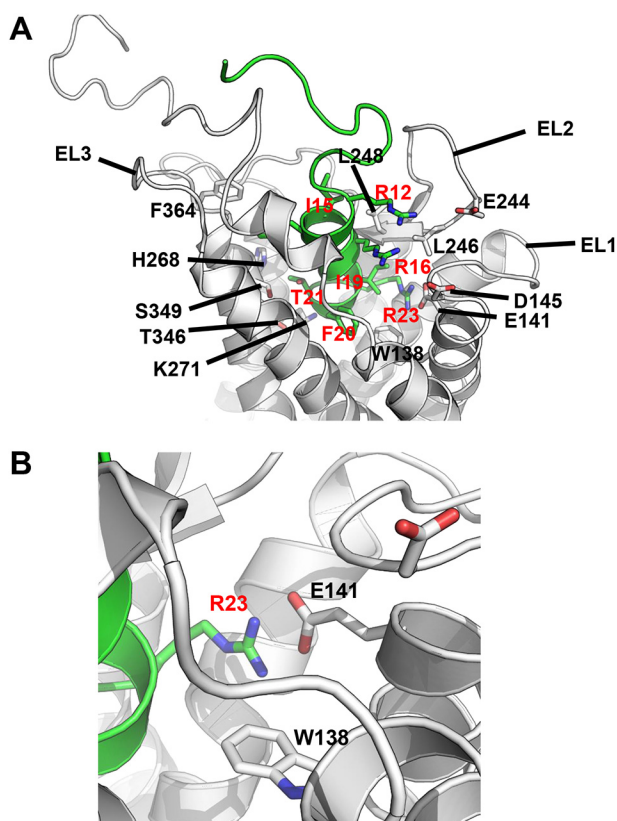
Figure 8. Antagonist R3 B1–22R binding site. *A*, an inactive-state homology model of RXFP3 docked with R3 B1–22R. R3 B1–22R is predicted to form a helix upon Arg[23] binding to RXFP3, allowing other binding amino acid residues to interact with counterpart amino acid residues in RXFP3. RXFP3 is *colored* in *gray*, with amino acid residues interacting with R3 B1–22R shown in *sticks* and *labeled* in *black*. Amino acid residues on R3 B1–22R involved in binding are shown in *sticks* and *labeled* in *red*. *B*, *close-up* interactions of Arg[23] with Glu[141] and Trp[138] on RXFP3, with Arg[23] sandwiched between Glu[141] and Trp[138] to form electrostatic and cation–π interactions with Glu[141] and Trp[138], respectively.

charged amino acid residue in RXFP3 as the key binding partner. However, no single acid residue mutation resulted in a total binding loss. Thus, we predicted that Arg[23] is making interactions with several amino acid residues, and with the guide of the inactive-state RXFP3 model and ligand docking, we postulate the binding site of Arg[23] to be sandwiched between Trp[138] and Glu[141] in TM2, forming both ionic and cation–π type interactions (Fig. 8*B*).

In relaxin-3, the B-chain helix ending at Cys[22] and the activation domain Arg[B26]-Trp[B27] are separated by a short linker

sequence, Gly-Gly-Ser. In contrast, in the antagonist, Arg[23] follows directly on the putative helical segment, which has several consequences for the binding. First, for the Arg[23] to reach into the binding pocket, the helix likely sits deeper in the transmembrane domains of RXFP3, which is possible for the smaller peptide lacking the A-chain. A few amino acid residues in TM5 (His[268]) and TM6 (Thr[346] and Ser[349]) affected R3 B1–22R binding but not relaxin-3 binding, which may be a result of this difference in positioning (Fig. 8). R3 B1–22R is a more potent antagonist as a peptide amide, with R3 B1–22R acid having a 10-fold lower affinity for RXFP3 (33). This is in contrast to relaxin-3, where the acid is favored. This can be explained by the fact that in relaxin-3, the longer tail allows the acid to potentially interact with Lys[271]; however, in the shorter tail of the antagonist, this interaction is not possible. Thus, the amide form, which does not require burying a charge that's not involved in an ionic interaction, is favored.

In summary, our current mutagenesis studies have led to refined models of relaxin-3 bound to an active-state model and R3 B1–22R bound to an inactive-state model of RXFP3 with improved accuracy and reliability. These data together with extensive mutagenesis data on R3 B1–22R in the companion article (59) have significantly improved our understanding of how relaxin-3 and R3 B1–22R interact with RXFP3. Such information is extremely valuable for structure-based drug design efforts to design next-generation RXFP3 agonists and antagonists.

Experimental procedures

Reagents

The RXFP3 full agonist analogue 2 and the antagonist R3 B1–22R were chemically prepared as described previously (33, 37). Eu-R3/I5, Eu-R3/I5, and Eu-labeled R3 B1–22R, Eu-H3B1–22R, were prepared as described previously (37, 48). Synthetic oligonucleotides were purchased from Sigma-Aldrich and are listed in Table S1. PCRs and cloning were undertaken as described previously (34). Delfia Enhancement Solution was purchased from PerkinElmer Life Sciences.

Mammalian cell culture

Human embryonic kidney 293T (HEK293T) cells (ATCC catalogue no. CRL-1573) were maintained in Dulbecco's modified Eagle's medium (DMEM; Gibco) supplemented with 10% fetal bovine serum (HyClone), 1% L-glutamine

(Gibco), and 1% penicillin/streptomycin (Gibco) in incubators at 37 °C, 5% CO_2, and 85% humidity. HEK293T cells were transfected with Lipofectamine®2000 (Thermo Fisher Scientific).

Site-directed mutagenesis

The forward and reverse primers for all mutants were designed with partially overlapping ends as described (49) and are listed in Table S1. Mutagenesis reactions on pcDNA3.1zeo (+) HA RXFP3 were performed using the method described previously (34). Individual mutants were screened and confirmed by DNA sequencing on both strands (Centre of Translational Pathology, University of Melbourne) to ensure that there were no introduced random mutations.

Homology modeling and docking

A model of RXFP3 with relaxin-3 docked into the binding site was prepared as described earlier (34) but using a different template for homology modeling. Briefly, the NMR solution structure of relaxin-3 (PDB entry 2FHW (28)) was used together with a homology model of RXFP3 based on the crystal structure of angiotensin II receptor in an activated state (PDB entry 5XJM (44)). Distance restraints corresponding to mutational data were introduced during the homology modeling procedure in Modeler 9v18 (50) to create an initial docking pose of relaxin-3 on RXFP3. The model was then embedded in a POPC/POPE/cholesterol membrane (60:20:20 relative composition) of dimensions 1.7×1.7 nm using the insane.py script (51) and the coarse-grained force field Martini version 2.0 (52). The system was then simulated for 500 ns to equilibrate the membrane using the Gromacs 2018.2 molecular dynamics engine (53). The system was then converted back to all-atom representation using an in-house modified version of the Backward algorithm (54). The system was then minimized and then equilibrated over 5 ns using the amber lipid17 and ff14SB force fields (55) and the molecular dynamics engine Amber18 (56). During the equilibration, the system was progressively heated up to 300 K with the protein heavy atoms restrained to their initial coordinates during the first 2.5 ns, and these restraints were then progressively removed over a 2.5-ns simulation time. The system was then simulated for 20 ns without restraints. The Langevin theromostat with a damping coefficient of 2.0 ps^{-1} and the Berendsen barostat with a coupling time constant of 1.0 ps were used to maintain pressure and temperature at 300 K and 1.0 bar, respectively. The root mean square deviation of the protein heavy atom coordinates to their initial position stabilized at 2.2 Å after a 4-ns simulation, suggesting that the system reached equilibrium.

A model of the antagonist bound to RXFP3 was generated similarly but using as a template for the receptor the X-ray structure of angiotensin I in an inactive state (PDB entry 4YAY (45)). The initial position of the antagonist was modeled manually with PyMOL version 2.0 (Schrödinger, LLC, New York) by considering the RXFP3/relaxin-3 binding mode, deleting the A-chain of relaxin-3, and repositioning the B-chain deeper in the binding pocket to satisfy the experimental data on the Arg[23] positioning. This model was then embedded in a membrane and refined using molecular dynamics simulation similarly as

the RXFP3/relaxin-3 model. The root mean square deviation of the protein heavy atom coordinates to their initial position stabilized at 2.9 Å after a 12-ns simulation, suggesting that the system reached equilibrium.

The final frames of the RXFP3/relaxin-3 and RXFP3/antagonist simulations were energy-minimized and used for interpreting mutational data. The resulting molecular models of the complexes have MolProbity scores (57) of 1.5 and 1.3, corresponding to the 96th and 98th percentile (100th percentile is the best), suggesting that the geometry of the models is excellent.

Agonist and antagonist whole-cell binding assays

HEK293T cells were plated out at 25,000 cells/well and were transfected in a 96-well ViewPlate (PerkinElmer Life Sciences) with plasmids encoding the constructs of interest (250 ng/well) and Eu-H3/I5 and Eu-R3 B1–22R binding assays conducted as described previously (34, 37, 48). Specific binding screening assays were performed using 5 nM Eu-R3/I5 in agonist-binding assays or 5 nM Eu-R3 B1–22R in antagonist-binding assays in the absence (total binding) and presence (nonspecific binding) of 1 μM unlabeled R3 B1–22R as described previously (34). Saturation binding assays were performed by preparing different concentrations of Eu-R3 B1–22R with (nonspecific binding) and without (total binding) competition of 1 μM unlabeled R3 B1–22R in 1% BSA in relaxin receptor binding buffer (20 mM HEPES, pH 7.5, 1.5 mM $CaCl_2$, 50 mM NaCl). Ligands were incubated for 90 min at room temperature and were then aspirated and washed with 200 μl/well cold PBS. 100 μl of Delfia Enhancement Solution was then added to each well, and the plate was shaken at 500 rpm for 15 min. The time-resolved fluorescence of europium was read on an Omega POLARstar (BMG Labtech) with the excitation/emission settings of 340 nm/615 nm. Specific binding was determined by subtracting the nonspecific binding from the total binding, and the graph was fitted to a one-site specific binding nonlinear regression. Each concentration point was performed in triplicate, and data were expressed as mean ± S.D. from at least three independent experiments. Significance was assessed using one-way analysis of variance (ANOVA) with Fisher's least significant difference (LSD) test on GraphPad Prism version 7.0 (GraphPad Software, La Jolla, CA).

Cell surface expression assays

All receptor constructs were expressed with a hemagglutinin (HA) epitope tag on the N terminus. HEK293T cells were plated at 200,000 cells/ml of DMEM in a 24-well plate (Costar) precoated with poly-L-lysine and transfected with 1 μg of plasmid DNA/well for 24 h as described previously (34). 24 h later, the media were aspirated, and cells were washed with Tris-buffered saline (TBS) solution (50 mM Tris, pH 7.4, 150 mM NaCl). Cells were then fixed with 3.7% formaldehyde in TBS for 20 min at room temperature, followed by two washes with TBS and subsequently blocked with 1% BSA/TBS for 30 min. The HA epitope tag was detected using a purified mouse monoclonal anti-HA, HA.11(16B12) (Covance), made up in a 1:1000 dilution in 1% BSA/TBS (400 μl/well) for 2 h at room temperature. The cells were washed and incubated with a 1:1000 dilution of

ASBMB

Alexa 488–conjugated goat anti-mouse IgG made up in 1% BSA/TBS (400 μl/well). Cells were then washed two times; 200 μl of lysis buffer (50 mM Tris, pH 7.4, 150 mM NaCl, 1 mM EDTA, 0.25% Triton X-100) was added to each well; and the plate was shaken for 15 min at 300 r.p.m. at room temperature. Cell lysates were then scraped, and 180 μl of cell lysates were transferred to a 96-well black Optiplate (Costar) to be read on Omega POLARstar (BMG Labtech) with excitation/emission wavelength of 490 nm/520 nm. Cell surface expression was determined by subtracting nonspecific binding of the antibody in cells transfected with pcDNA3.1 (+) zeo and divided by the HA-RXFP3 WT expression to get a percentage HA-RXFP3 expression. Significance was assessed using one-way ANOVA with Fisher's LSD test on GraphPad Prism version 7.0.

cAMP activity assays

HEK293T cells were plated at 25,000 cells/well in a 96-well CellBind plate (Corning) and co-transfected the next day with plasmid encoding various RXFP3 receptor constructs and pCRE β-gal as a cAMP-response element (CRE)-controlled reporter of cAMP activity (58). 24 h post-transfection, medium was removed, and increasing concentrations of the RXFP3 full agonist, analogue 2 (37), made up in DMEM containing 500 nM forskolin were added to the respective wells. The stimulation was carried out for 6 h at 37 °C, 5% CO_2, after which medium was aspirated and plates were kept frozen at −80 °C until further analysis. Development of the plates required the plates and assay buffers to be first thawed to room temperature. 25 μl of assay buffer 1 (100 mM Na_2HPO_4, pH 8.0, 2 mM $MgSO_4$, and 0.1 mM $MnCl_2$) was added into each well and shaken at room temperature for 10 min before adding 100 μl of assay buffer 2 (similar to buffer 1 with the addition of 0.5% Triton X-100 and 40 mM β-mercaptoethanol) into each well and further shaken for 10 min at room temperature. 25 μl of substrate for β-gal, chlorophenol red β-D-galactopyranoside (Roche Applied Science), was added into each well with shaking until color change was observed. The plate was then read and absorbance was measured at 570 nm on a Bio-Rad plate reader. Readings were normalized to medium containing 500 nM forskolin (positive control) as 100% and to medium only (negative control) as 0%. Normalized data were fitted to a nonlinear regression sigmoidal dose-response curve on GraphPad Prism version 6.0. Each concentration point was performed in triplicates, and the data were expressed as mean ± S.E. from at least three independent experiments. pEC_{50} values of each mutant construct were subjected to one-way ANOVA with Fisher's LSD test on GraphPad Prism version 7.0.

References

1. Bathgate, R. A., Samuel, C. S., Burazin, T. C. D., Layfield, S., Claasz, A. A., Reytomas, I. G. T., Dawson, N. F., Zhao, C., Bond, C., Summers, R. J., Parry, L. J., Wade, J. D., and Tregear, G. W. (2002) Human relaxin gene 3 (H3) and the equivalent mouse relaxin (M3) gene: novel members of the relaxin peptide family. *J. Biol. Chem.* **277,** 1148–1157 CrossRef Medline
2. Wilkinson, T. N., Speed, T. P., Tregear, G. W., and Bathgate, R. A. (2005) Evolution of the relaxin-like peptide family. *BMC Evol. Biol.* **5,** 14 CrossRef Medline
3. Bathgate, R. A., Ivell, R., Sanborn, B. M., Sherwood, O. D., and Summers, R. J. (2006) International Union of Pharmacology LVII: recommendations for the nomenclature of receptors for relaxin family peptides. *Pharmacol. Rev.* **58,** 7–31 CrossRef Medline
4. Bedarkar, S., Turnell, W. G., Blundell, T. L., and Schwabe, C. (1977) Relaxin has conformational homology with insulin. *Nature* **270,** 449–451 CrossRef Medline
5. Rosengren, K. J., Bathgate, R. A., Craik, D. J., Daly, N. L., Haugaard-Jönsson, L. M., Hossain, M. A., and Wade, J. D. (2009) Structural insights into the function of relaxins. *Ann. N.Y. Acad. Sci.* **1160,** 20–26 CrossRef Medline
6. Liu, C., Eriste, E., Sutton, S., Chen, J., Roland, B., Kuei, C., Farmer, N., Jörnvall, H., Sillard, R., and Lovenberg, T. W. (2003) Identification of relaxin-3/INSL7 as an endogenous ligand for the orphan G-protein-coupled receptor GPCR135. *J. Biol. Chem.* **278,** 50754–50764 CrossRef Medline
7. Matsumoto, M., Kamohara, M., Sugimoto, T., Hidaka, K., Takasaki, J., Saito, T., Okada, M., Yamaguchi, T., and Furuichi, K. (2000) The novel G-protein coupled receptor SALPR shares sequence similarity with somatostatin and angiotensin receptors. *Gene* **248,** 183–189 CrossRef Medline
8. Sudo, S., Kumagai, J., Nishi, S., Layfield, S., Ferraro, T., Bathgate, R. A., and Hsueh, A. J. W. (2003) H3 relaxin is a specific ligand for LGR7 and activates the receptor by interacting with both the ectodomain and the exoloop 2. *J. Biol. Chem.* **278,** 7855–7862 CrossRef Medline
9. Liu, C., Chen, J., Sutton, S., Roland, B., Kuei, C., Farmer, N., Sillard, R., and Lovenberg, T. W. (2003) Identification of relaxin-3/INSL7 as a ligand for GPCR142. *J. Biol. Chem.* **278,** 50765–50770 CrossRef Medline
10. Chen, J., Kuei, C., Sutton, S. W., Bonaventure, P., Nepomuceno, D., Eriste, E., Sillard, R., Lovenberg, T. W., and Liu, C. (2005) Pharmacological characterization of relaxin-3/INSL7 receptors GPCR135 and GPCR142 from different mammalian species. *J. Pharmacol. Exp. Ther.* **312,** 83–95 Medline
11. Donizetti, A., Fiengo, M., Minucci, S., and Aniello, F. (2009) Duplicated zebrafish relaxin-3 gene shows a different expression pattern from that of the co-orthologue gene. *Dev. Growth Differ.* **51,** 715–722 CrossRef Medline
12. Burazin, T. C. D., Bathgate, R. A., Macris, M., Layfield, S., Gundlach, A. L., and Tregear, G. W. (2002) Restricted, but abundant, expression of the novel rat gene-3 (R3) relaxin in the dorsal tegmental region of brain. *J. Neurochem.* **82,** 1553–1557 CrossRef Medline
13. Ma, S., Sang, Q., Lanciego, J. L., and Gundlach, A. L. (2009) Localization of relaxin-3 in brain of *Macaca fascicularis*: identification of a nucleus incertus in primate. *J. Comp. Neurol.* **517,** 856–872 CrossRef Medline
14. Ma, S., Shen, P. J., Sang, Q., Lanciego, J. L., and Gundlach, A. L. (2009) Distribution of relaxin-3 mRNA and immunoreactivity and RXFP3-binding sites in the brain of the macaque, *Macaca fascicularis. Ann. N.Y. Acad. Sci.* **1160,** 256–258 CrossRef Medline
15. Ma, S., Bonaventure, P., Ferraro, T., Shen, P. J., Burazin, T. C. D., Bathgate, R. A., Liu, C., Tregear, G. W., Sutton, S. W., and Gundlach, A. L. (2007) Relaxin-3 in GABA projection neurons of nucleus incertus suggests widespread influence on forebrain circuits via G-protein-coupled receptor-135 in the rat. *Neuroscience* **144,** 165–190 CrossRef Medline
16. McGowan, B. M. C., Stanley, S. A., Ghatei, M. A., and Bloom, S. R. (2009) Relaxin-3 and its role in neuroendocrine function. *Ann. N.Y. Acad. Sci.* **1160,** 250–255 CrossRef Medline

17. Sutton, S. W., Bonaventure, P., Kuei, C., Roland, B., Chen, J., Nepomuceno, D., Lovenberg, T. W., and Liu, C. (2004) Distribution of G-protein-coupled receptor (GPCR)135 binding sites and receptor mRNA in the rat brain suggests a role for relaxin-3 in neuroendocrine and sensory processing. *Neuroendocrinology* **80,** 298–307 CrossRef Medline

18. Smith, C. M., Shen, P. J., Banerjee, A., Bonaventure, P., Ma, S., Bathgate, R. A., Sutton, S. W., and Gundlach, A. L. (2010) Distribution of relaxin-3 and RXFP3 within arousal, stress, affective, and cognitive circuits of mouse brain. *J. Comp. Neurol.* **518,** 4016–4045 CrossRef Medline

19. Ma, S., Olucha-Bordonau, F. E., Hossain, M. A., Lin, F., Kuei, C., Liu, C., Wade, J. D., Sutton, S. W., Nuñez, A., and Gundlach, A. L. (2009) Modulation of hippocampal θ oscillations and spatial memory by relaxin-3 neurons of the nucleus incertus. *Learn. Mem.* **16,** 730–742 CrossRef Medline

20. Banerjee, A., Shen, P. J., Ma, S., Bathgate, R. A., and Gundlach, A. L. (2010) Swim stress excitation of nucleus incertus and rapid induction of relaxin-3 expression via CRF1 activation. *Neuropharmacology* **58,** 145–155 CrossRef Medline

21. Watanabe, Y., Tsujimura, A., Takao, K., Nishi, K., Ito, Y., Yasuhara, Y., Nakatomi, Y., Yokoyama, C., Fukui, K., Miyakawa, T., and Tanaka, M. (2011) Relaxin-3-deficient mice showed slight alteration in anxiety-related behavior. *Front. Behav. Neurosci.* **5,** 50 Medline

22. McGowan, B. M., Stanley, S. A., Smith, K. L., Minnion, J. S., Donovan, J., Thompson, E. L., Patterson, M., Connolly, M. M., Abbott, C. R., Small, C. J., Gardiner, J. V., Ghatei, M. A., and Bloom, S. R. (2006) Effects of acute and chronic relaxin-3 on food intake and energy expenditure in rats. *Regul. Pept.* **136,** 72–77 CrossRef Medline

23. Ryan, P. J., Kastman, H. E., Krstew, E. V., Rosengren, K. J., Hossain, M. A., Churilov, L., Wade, J. D., Gundlach, A. L., and Lawrence, A. J. (2013) Relaxin-3/RXFP3 system regulates alcohol-seeking. *Proc. Natl. Acad. Sci. U.S.A.* **110,** 20789–20794 CrossRef Medline

24. Patil, N. A., Rosengren, K. J., Separovic, F., Wade, J. D., Bathgate, R. A. D., and Hossain, M. A. (2017) Relaxin family peptides: structure-activity relationship studies. *Br. J. Pharmacol.* **174,** 950–961 CrossRef Medline

25. Hossain, M. A., Rosengren, K. J., Haugaard-Jönsson, L. M., Zhang, S., Layfield, S., Ferraro, T., Daly, N. L., Tregear, G. W., Wade, J. D., and Bathgate, R. A. (2008) The A-chain of human relaxin family peptides has distinct roles in the binding and activation of the different relaxin family peptide receptors. *J. Biol. Chem.* **283,** 17287–17297 CrossRef Medline

26. Liu, C., Chen, J., Kuei, C., Sutton, S., Nepomuceno, D., Bonaventure, P., and Lovenberg, T. W. (2005) Relaxin-3/insulin-like peptide 5 chimeric peptide, a selective ligand for G protein-coupled receptor (GPCR)135 and GPCR142 over leucine-rich repeat-containing G protein-coupled receptor 7. *Mol. Pharmacol.* **67,** 231–240 CrossRef Medline

27. Haugaard-Jönsson, L. M., Hossain, M. A., Daly, N. L., Bathgate, R. A., Wade, J. D., Craik, D. J., and Rosengren, K. J. (2008) Structure of the R3/I5 chimeric relaxin peptide, a selective GPCR135 and GPCR142 agonist. *J. Biol. Chem.* **283,** 23811–23818 CrossRef Medline

28. Rosengren, K. J., Lin, F., Bathgate, R. A., Tregear, G. W., Daly, N. L., Wade, J. D., and Craik, D. J. (2006) Solution structure and novel insights into the determinants of the receptor specificity of human relaxin-3. *J. Biol. Chem.* **281,** 5845–5851 CrossRef Medline

29. Hojo, K., Hossain, M. A., Tailhades, J., Shabanpoor, F., Wong, L. L. L., Ong-Pålsson, E. E. K., Kastman, H. E., Ma, S., Gundlach, A. L., Rosengren, K. J., Wade, J. D., and Bathgate, R. A. (2016) Development of a single-chain peptide agonist of the relaxin-3 receptor using hydrocarbon stapling. *J. Med. Chem.* **59,** 7445–7456 CrossRef Medline

30. Jayakody, T., Marwari, S., Lakshminarayanan, R., Tan, F. C. K., Johannes, C. W., Dymock, B. W., Poulsen, A., Herr, D. R., and Dawe, G. S. (2016) Hydrocarbon stapled B chain analogues of relaxin-3 retain biological activity. *Peptides* **84,** 44–57 CrossRef Medline

31. Kuei, C., Sutton, S., Bonaventure, P., Pudiak, C., Shelton, J., Zhu, J., Nepomuceno, D., Wu, J., Chen, J., Kamme, F., Seierstad, M., Hack, M. D., Bathgate, R. A., Hossain, M. A., Wade, J. D., *et al.* (2007) R3(BΔ23 27)R/I5 chimeric peptide, a selective antagonist for GPCR135 and GPCR142 over relaxin receptor LGR7: *in vitro* and *in vivo* characterization. *J. Biol. Chem.* **282,** 25425–25435 CrossRef Medline

32. Hossain, M. A., Bathgate, R. A., Rosengren, K. J., Shabanpoor, F., Zhang, S., Lin, F., Tregear, G. W., and Wade, J. D. (2009) The structural and functional role of the B-chain C-terminal arginine in the relaxin-3 peptide antagonist, R3(BΔ23–27)R/I5. *Chem. Biol. Drug Des.* **73,** 46–52 CrossRef Medline

33. Haugaard-Kedström, L. M., Shabanpoor, F., Hossain, M. A., Clark, R. J., Ryan, P. J., Craik, D. J., Gundlach, A. L., Wade, J. D., Bathgate, R. A., and Rosengren, K. J. (2011) Design, synthesis, and characterization of a single-chain peptide antagonist for the relaxin-3 receptor RXFP3. *J. Am. Chem. Soc.* **133,** 4965–4974 CrossRef Medline

34. Bathgate, R. A., Oh, M. H. Y., Ling, W. J. J., Kaas, Q., Hossain, M. A., Gooley, P. R., and Rosengren, K. J. (2013) Elucidation of relaxin-3 binding interactions in the extracellular loops of RXFP3. *Front. Endocrinol. (Lausanne)* **4,** 13 CrossRef Medline

35. Zhang, W. J., Wang, X. Y., Guo, Y. Q., Luo, X., Gao, X. J., Shao, X. X., Liu, Y. L., Xu, Z. G., and Guo, Z. Y. (2014) The highly conserved negatively charged Glu141 and Asp145 of the G-protein-coupled receptor RXFP3 interact with the highly conserved positively charged arginine residues of relaxin-3. *Amino Acids* **46,** 1393–1402 CrossRef Medline

36. Hu, M. J., Shao, X. X., Wang, J. H., Wei, D., Liu, Y. L., Xu, Z. G., and Guo, Z. Y. (2016) Identification of hydrophobic interactions between relaxin-3 and its receptor RXFP3: implication for a conformational change in the B-chain C-terminus during receptor binding. *Amino Acids* **48,** 2227–2236 CrossRef Medline

37. Shabanpoor, F., Akhter Hossain, M., Ryan, P. J., Belgi, A., Layfield, S., Kocan, M., Zhang, S., Samuel, C. S., Gundlach, A. L., Bathgate, R. A., Separovic, F., and Wade, J. D. (2012) Minimization of human relaxin-3 leading to high-affinity analogues with increased selectivity for relaxin-family peptide 3 receptor (RXFP3) over RXFP1. *J. Med. Chem.* **55,** 1671–1681 CrossRef Medline

38. Ballesteros, J. A., and Weinstein, H. (1995) Integrated methods for the construction of three-dimensional models and computational probing of structure-function relations in G protein-coupled receptors. *Methods Neurosci.* **25,** 366–428 CrossRef

39. Ahuja, S., and Smith, S. O. (2009) Multiple switches in G protein-coupled receptor activation. *Trends Pharmacol. Sci.* **30,** 494–502 CrossRef Medline

40. Hulme, E. C. (2013) GPCR activation: a mutagenic spotlight on crystal structures. *Trends Pharmacol. Sci.* **34,** 67–84 CrossRef Medline

41. Stoddart, L. A., Kellam, B., Briddon, S. J., and Hill, S. J. (2014) Effect of a toggle switch mutation in TM6 of the human adenosine A_3 receptor on G_i protein-dependent signalling and G_i-independent receptor internalization. *Br. J. Pharmacol.* **171,** 3827–3844 CrossRef Medline

42. Holst, B., Nygaard, R., Valentin-Hansen, L., Bach, A., Engelstoft, M. S., Petersen, P. S., Frimurer, T. M., and Schwartz, T. W. (2010) A conserved aromatic lock for the tryptophan rotameric switch in TM-VI of seven-transmembrane receptors. *J. Biol. Chem.* **285,** 3973–3985 CrossRef Medline

43. Wu, B., Chien, E. Y. T., Mol, C. D., Fenalti, G., Liu, W., Katritch, V., Abagyan, R., Brooun, A., Wells, P., Bi, F. C., Hamel, D. J., Kuhn, P., Handel, T. M., Cherezov, V., and Stevens, R. C. (2010) Structures of the CXCR4 chemokine receptor in complex with small molecule and cyclic peptide antagonists. *Science* **330,** 1066–1071 CrossRef Medline

44. Asada, H., Horita, S., Hirata, K., Shiroishi, M., Shiimura, Y., Iwanari, H., Hamakubo, T., Shimamura, T., Nomura, N., Kusano-Arai, O., Uemura, T., Suno, C., Kobayashi, T., and Iwata, S. (2018) Crystal structure of the human angiotensin II type 2 receptor bound to an angiotensin II analog. *Nat. Struct. Mol. Biol.* **25,** 570–576 CrossRef Medline

45. Zhang, H., Unal, H., Gati, C., Han, G. W., Liu, W., Zatsepin, N. A., James, D., Wang, D., Nelson, G., Weierstall, U., Sawaya, M. R., Xu, Q., Messerschmidt, M., Williams, G. J., Boutet, S., *et al.* (2015) Structure of the angiotensin receptor revealed by serial femtosecond crystallography. *Cell* **161,** 833–844 CrossRef Medline

46. Wang, X. Y., Guo, Y. Q., Zhang, W. J., Shao, X. X., Liu, Y. L., Xu, Z. G., and Guo, Z. Y. (2014) The electrostatic interactions of relaxin-3 with receptor RXFP4 and the influence of its B-chain C-terminal conformation. *FEBS J.* **281,** 2927–2936 CrossRef Medline

47. Shabanpoor, F., Bathgate, R. A., Wade, J. D., and Hossain, M. A. (2013) C-terminus of the B-chain of relaxin-3 is important for receptor activity. *PLoS One* **8,** e82567 CrossRef Medline

ASBMB

48. Haugaard-Kedström, L. M., Wong, L. L. L., Bathgate, R. A., and Rosengren, K. J. (2015) Synthesis and pharmacological characterization of a europium-labelled single-chain antagonist for binding studies of the relaxin-3 receptor RXFP3. *Amino Acids* **47,** 1267–1271 CrossRef Medline

49. Liu, H., and Naismith, J. H. (2008) An efficient one-step site-directed deletion, insertion, single and multiple-site plasmid mutagenesis protocol. *BMC Biotechnol.* **8,** 91 CrossRef Medline

50. Sali, A., and Blundell, T. L. (1993) Comparative protein modelling by satisfaction of spatial restraints. *J. Mol. Biol.* **234,** 779–815 CrossRef Medline

51. Wassenaar, T. A., Ingólfsson, H. I., Böckmann, R. A., Tieleman, D. P., and Marrink, S. J. (2015) Computational lipidomics with insane: a versatile tool for generating custom membranes for molecular simulations. *J. Chem. Theory Comput.* **11,** 2144–2155 CrossRef Medline

52. Marrink, S. J., Risselada, H. J., Yefimov, S., Tieleman, D. P., and de Vries, A. H. (2007) The MARTINI force field: coarse grained model for biomolecular simulations. *J. Phys. Chem. B* **111,** 7812–7824 CrossRef Medline

53. Abraham, M. J., Murtola, T., Schulz, R., Páll, S., Smith, J. C., Hess, B., and Lindahl, E. (2015) GROMACS: high performance molecular simulations through multi-level parallelism from laptops to supercomputers. *SoftwareX* **1,** 19–25

54. Wassenaar, T. A., Pluhackova, K., Böckmann, R. A., Marrink, S. J., and Tieleman, D. P. (2014) Going backward: a flexible geometric approach to reverse transformation from coarse grained to atomistic models. *J. Chem. Theory Comput.* **10,** 676–690 CrossRef Medline

55. Dickson, C. J., Madej, B. D., Skjevik, A. A., Betz, R. M., Teigen, K., Gould, I. R., and Walker, R. C. (2014) Lipid14: the amber lipid force field. *J. Chem. Theory Comput.* **10,** 865–879 CrossRef Medline

56. Case, D. A., Ben-Shalom, I. Y., Brozell, S. R., Cerutti, D. S., Cheatham, T. E., 3rd, Cruzeiro, V. W. D., Darden, T. A., Duke, R. E., Ghoreishi, D., Gilson, M. K., Gohlke, H., Goetz, A. W., Greene, D., Harris, R., Homeyer, N., Izadi, S., Kovalenko, A., and Kurtzman, T. P. (2018) *Amber 2018*, University of California, San Francisco

57. Williams, C. J., Headd, J. J., Moriarty, N. W., Prisant, M. G., Videau, L. L., Deis, L. N., Verma, V., Keedy, D. A., Hintze, B. J., Chen, V. B., Jain, S., Lewis, S. M., Arendall, W. B., 3rd, Snoeyink, J., Adams, P. D., *et al.* (2018) MolProbity: more and better reference data for improved all-atom structure validation. *Protein Sci.* **27,** 293–315 CrossRef Medline

58. Chen, W., Shields, T. S., Stork, P. J., and Cone, R. D. (1995) A colorimetric assay for measuring activation of G_s- and G_q-coupled signaling pathways. *Anal. Biochem.* **226,** 349–354 CrossRef Medline

59. Haugaard-Kedström, L. M., Lee, H. S., Jones, M. V., Song, A., Rathod, V., Hossain, M. A., Bathgate, R. A. D., and Rosengren, K. J. (2018) Binding conformation and determinants of a single-chain peptide antagonist at the relaxin-3 receptor RXFP3. *J. Biol. Chem.* **293,** 15765–15776 CrossRef Medline

Distinct but overlapping binding sites of agonist and antagonist at the relaxin family peptide 3 (RXFP3) receptor

Lilian L. L. Wong, Daniel James Scott, Mohammed Akhter Hossain, Quentin Kaas, K. Johan Rosengren and Ross A. D. Bathgate

Access the most updated version of this article at doi: 10.1074/jbc.RA118.002645

Alerts:
- When this article is cited
- When a correction for this article is posted

Click here to choose from all of JBC's e-mail alerts

This article cites 58 references, 16 of which can be accessed free at
http://www.jbc.org/content/293/41/15777.full.html#ref-list-1